TU Delft
Delft University of Technology

Faculty of Civil Engineering and Geosciences
Department of Hydraulic and Geotechnical Engineering
Fluid Mechanics Section

Survey of the numerical characterisation of 2-D complex clusters

Federico Maggi
Report no. 4-02

2002

TUDelft

Technische Universiteit Delft

Environmental Fluidmechanics Section, Faculty of Civil Engineering and Geosciences, Delft University of Technology, P.O. Box 5048, 2600 GA, The Netherlands. Tel. +31 15 278 4070; Fax +31 15 278 59 75; E-mail: f.maggi@ct.tudelft.nl

Survey of the numerical characterisation of 2-D complex clusters

Federico Maggi

June 26, 2003

Hydromechanics Section, Faculty of Civil Engineering and Geosciences, Delft University of Technology, P.O. Box 5048, 2600 GA, The Netherlands. Tel. +31 15 278 4070; Fax +31 15 278 59 75; E-mail: F.Maggi@ct.tudelft.nl

1

Contents

1   Introduction to complex systems

The study of cluster formation is common in many fields of science and technology (aerosols, colloidal suspensions, hetero-disperse particulate systems in general, growth processes far from equilibrium, etc.). The term "cluster" is a general word indicating an object consisting of a set of elementary unites organised with a certain structure. In our research, a cluster is an aggregate (floc) of cohesive sediments formed in a turbulent environment from a number of primary particles consisting of clay minerals. The geometric characterisation of a cluster is important to distinguish different features of the object under study. One of the most important aspects of real and artificial clusters is their fractal nature, that is their capability to occupy their own volume. From this point of view, many investigations have been performed about geometrical features (size, volume, density, permeability and porosity properties, etc.) and dynamical features (growth processes, pattern formation, equilibrium).

When studying a multi-disperse system consisting of cohesive particles diluted in a fluid in a regime of turbulence, two main processes can be identified in the process of cluster formation: *aggregation* and *break-up*. A large amount of studies in the past tried to establish the correlations between the global variables of a system (particle concentration, turbulence shear rate, chemicals presence, viscosity of the medium, etc.) and the average characteristics of the clusters (size, volume, strength, settling velocity, etc.). An indirect interpretation of the aggregation and break-up processes could be achieved from those characterisations. Many studies showed relations between different quantities; DYER (1989), for example, investigated the relation between sediment concentration, floc size and turbulence shear rate; WINTERWERP (1999) focused on the Lagrangian growth of mud flocs; KRANENBURG (1998) found an analytical formulation to evaluate the floc strength on the basis of rheological measurements, etc. At the same time, many efforts have been spent to investigate the properties of individual clusters from a physical and mathematical point of view by means of numerical simulations. In those studies the focus was on the dynamical process of cluster formation by means of random numbers generators. Different models resulted from those investigations; in particular, VICSEK (1992) analysed fractal DLA (Diffusion Limited Aggregation) and CCA (Cluster Cluster Aggregation) growth processes; MEAKIN (1998) studied the scaling rules of cluster formation far from equilibrium and the fractal characterisation of such clusters, and many studies are still being carried out in different fields.

Evidence of the impact of the environment on cluster (or floc) formation has been found from experimental investigations on cohesive sedimentary suspensions: for example, a highly turbulent medium produces small spherical-shaped flocs with high fractal dimensions, while a low-turbulent medium produces chain-like flocs with low fractal dimensions, WELLS AND GOLDBERG (1993). At the same time, numerical evidence has been found about the impact that the structural organisation of growing clusters has on the growth itself. For this reason, it is natural to look at the possibility to establish a correlation between the dynamical processes of growth/break-up in a given environment and the internal organisation of a fractal cluster. Moreover, from the characterisation of the environment in which a cluster grows, is likely to induce some characteristics of the clusters themselves and, vice versa, from the structural properties of individual cluster it is possible to deduce some kinematical and dynamical processes which controle the growth of the cluster. In practice, a feed-back exists between the kinematic and dynamics of aggregation/break-up (processes within and by means of the environment) and the organisation of the cluster (that is a local and individual feature).

Studies in biology by MATURANA AND VARELA (1972) showed that forms of organisation arise in systems subject to negative feed-back; NICOLIS AND PRIGOGINE (1974) investigated

5

the spontaneous onset of organisation in chemical reactions far from equilibrium, while VIC-SEK (1992) and MEAKIN (1998) observed spontaneous fractal organisation in particulate systems. These issues lead us to look at flocs as fractal structures that grow and break-up within a population, continuously in time, under conditions far from equilibrium and in a feed-back system with self-organisation properties.

2 Introduction to fractal geometry

A fractal is an object which possesses a dimension $d \leq d_E$, where d_E is the Euclidean dimension of the space (support) which envelops the fractal. In the last three decades, the development of digital computing has given a strong pulse to the investigation of fractals. Thanks to this, it has been possible to collect a large amount of information about the properties of fractals from numerical simulations. In this section we collect some of the features of fractal sets in order to draw a hierarchic tree of classification of fractals. This work will help the reader to understand the subsequent sections of the report.

2.1 Characteristics of fractal objects and classification

Fractals are fragmented geometric-shaped sets that can be subdivided into parts, each of which is (at least approximately) a copy of the whole. They show a high degree of geometrical complexity which can reproduce by analogy many natural object. Fractal objects defy the conventional topological measures and are characterised by a non-integer value of their dimension; such non-integer value is referred to as *fractal dimension* and, in a way, it is the only quantitative measure to identify a fractal.

The fractal dimension strictly lies between the topological dimension d_T (the dimension of the set which constitute it.[1]) and the Euclidian dimension d_E (the dimension of the support[2].).

From the beginning of the 20th century, many scientists, like Peano (1858-1932) and Hausdorff (1869-1942), spent many efforts in investigating objects which have a dimension greater than the corresponding topological dimension (see for example the Peano curve). In the course of time, different approaches led to different definitions of fractal dimensions. For this reason, some authors now prefer to refer to the concept of *fractal dimensionality* more than *fractal dimension*, keeping in mind that all the fractal dimensionalities are fractal dimensions because they are non-integer numbers.

We attempt to classify fractals in a hierarchic structure, starting from the "large-scale" down to the "small-scale" properties. We report also examples of each of the hierarchical branches in order to help the reader to figure out the various properties.

Fractals can be *artificial* (ART) or *real* (REA). Artificial are all the fractal non present in nature, while real are the fractals recorded, for example, by imaging techniques. Artificial fractals can be *deterministic* (DET) or *random* (RND). Deterministic fractals are obtained by applying recursive functions (IFS, Iterated Function Systems) consisting of adding or subdividing a set reiteratively, while random fractals are obtained by means of random number generators[3]. At a lower level, fractals can be classified as *fully self-similar* (FSS) or *statistically self-similar* (SSS). Self-similarity is a widely discussed (and sometimes misunderstood) property of fractals. Only regular and deterministic fractals have a fully self-similar structure at different scales, Meakin (1998). In most of the cases, like experimental measurements or random-generated fractals, self-similarity is only apparent; that is, the patterns at different

---

[1]For instance: a point in space has a dimension $d_T = 0$, a curve corresponds to a $d_T = 1$, a surface to $d_T = 2$, etc.

[2]For instance: a plane has a Euclidian dimension $d_E = 2$, a volume has a $d_E = 3$, etc.

[3]Simulated random fractals are normally associated with real fractals but a distinction has to be made with respect to the use of the terms. Real fractals often show a complex structure which is the result of a "certain amount" of determinism and a "certain amount" of randomness. Random number generators in digital computing are based on deterministic algorithms. Therefore, simulated random fractals cannot be considered identically as stochastic fractals, but an approximation.

scales only look like each other but, in detail, they do not have the same structure. These fractals are called statistically self-similar. Deterministic fractals can be both FSS and SSS, while random fractals are intrinsically SSS.

Real fractals (REA) can show full and statistical self-similarity properties as well, but the largest part of natural fractals show only a small range of scales in which they can be considered FSS. Therefore we say that real fractals are statistically self-similar. FSS fractals can be *fully homogeneous* (FHO) or *inhomogeneous* (or *statistically homogeneous* or *heterogeneous*) (SHO).
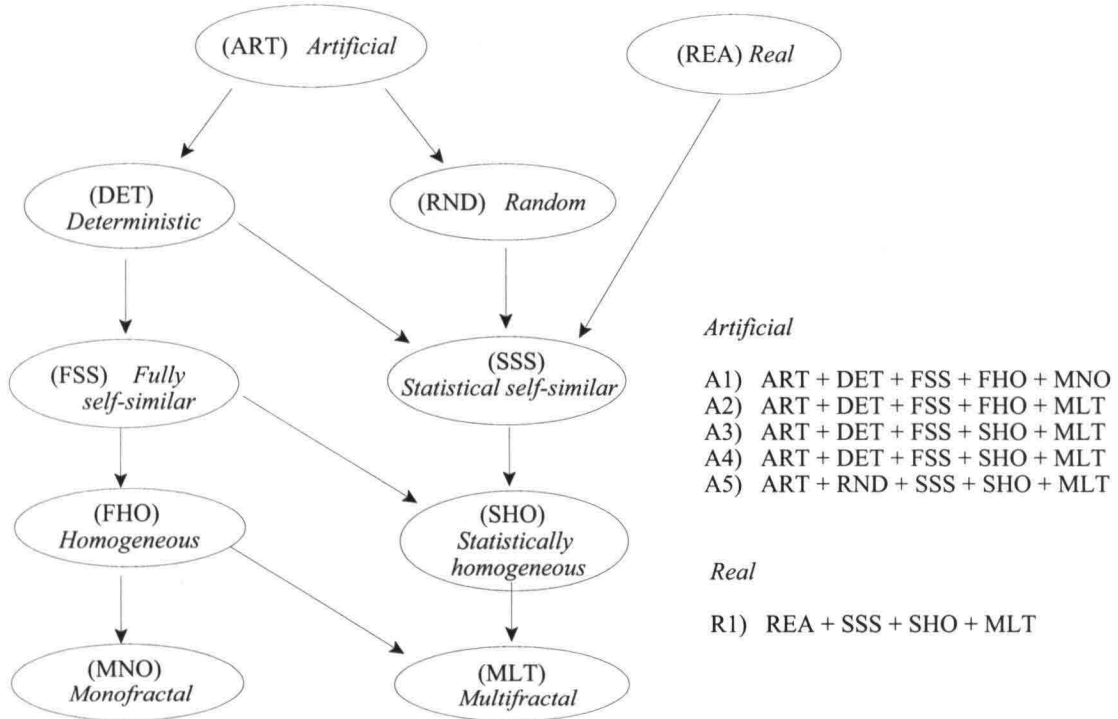

Artificial

A1) ART + DET + FSS + FHO + MNO
A2) ART + DET + FSS + FHO + MLT
A3) ART + DET + FSS + SHO + MLT
A4) ART + DET + FSS + SHO + MLT
A5) ART + RND + SSS + SHO + MLT

Real

R1) REA + SSS + SHO + MLT

Figure 1: *Hierarchical classification of fractals.*

For example, deterministic FSS and FHO fractals are well known in literature, like the Koch curve or the Sierpinsky carpet. They can be built also in such a way to have inhomogeneity by applying the iterative function a different number of times at different regions of the fractal, MEAKIN (1998). SSS fractals show homogeneity only in a small range of different scales and therefore they can be classified as inhomogeneous. An example is given by growing fractals in the regime of DLA (Diffusion Limited Aggregation). According to recent investigations, MEAKIN (1998) observed a progressive space filling ability of the structure of a cluster growing in DLA regime. This corresponds to slight increases in fractal dimension and a consequent loss of self-similarity.

The last hierarchical step is the *monofractal* (MNO) and *multifractal* (MLT) nature of fractal sets. Deterministic FSS and FHO fractals possess only one fractal dimension, while all the other fractal sets are multifractals because of the presence of a spectrum of fractal dimensionalities. A representation of such hierarchic classification is shown in Figure 1, while examples of the classes of fractals represented within this tree are collected in Figure 2 - Figure 7.
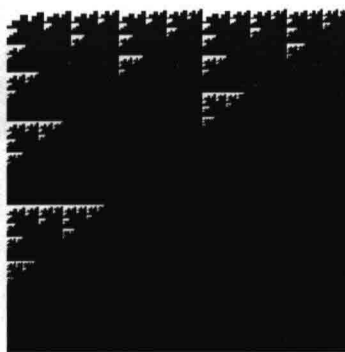
8

Figure 2: *A1-class reiterative fractal.*

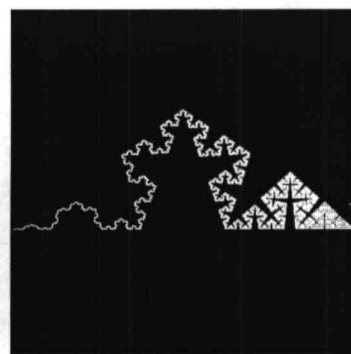Figure 3: *A2-class 2-D 2-scales Cantor set,* MACH ET AL. (1995).

Figure 4: *A3-class Kock curve,* MEAKIN (1998).

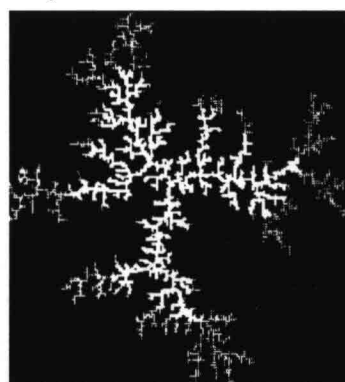Figure 5: *A4-class Ikeda map,* IKEDA ET AL. (1980).

Figure 6: *A5-class DLA aggregate,* VICSEK (1992).

Figure 7: *R1-class kaolinite aggregate, optical measurements.*

The fractal $A1$ in Figure 2 is a DET FSS FHO and MNO fractal obtained by an additive iteration function. The fractal $A2$ in Figure 3 is a DET FSS FHO MLT 2-D 2-scale Cantor set investigated by MACH ET AL (1995). The fractal $A3$ in Figure 4 is a DET FSS SHO and MLT Koch curve obtained as reported in MEAKIN (1998). The fractal $A4$ in Figure 5 is DET SSS SHO MLT fractal representing the strange attractor of the chaotic dynamic of the Ikeda equations, called Iked map, IKEDA ET AL. (1980). $A5$ in Figure 6 is a RND SSS SHO and MLT fractal obtained by aggregation of elementary particles in a DLA regime, VICSEK (1992). Finally, the fractal $R1$ in Figure 7 is a REA SSS SHO and MLT obtained by digital grabbing of a real aggregate made from kaolinite particles.

2.2 Fractal dimensions

Fractals, as already mentioned, have a non-integer dimension normally referred to as *fractal dimension*. The term fractal dimension means, in fact, that the object under investigation does not fill its Euclidian space fully or, in analogy, that the object occupies a space dimensionally greater than its topological space. Mandelbrot (1983) defines fractals as:

> *[a fractal is]...a point-set for which the so colled Hausdorff-Besicovitch dimension is strictly greater than the topological dimension.*

9

It is worth while to define the Hausdorff-Besicovitch dimension. To do this we pass through the Hausdorff measure in order to establish the knowledge required to understand other fractal dimensions as well as to give an indication of the difficulty involved in the calculation of this dimension. Let us consider a set $\Lambda \epsilon R^n$: the diameter of Λ is defined as the greatest distance between any two points $\mathbf{p}_i$ and $\mathbf{p}_j$ in Λ:

$$|\Lambda| = \sup\{|\mathbf{p}_i - \mathbf{p}_j| : \mathbf{p}_i, \mathbf{p}_j \epsilon R^n\}. \tag{1}$$

For a given $\delta > 0$ we can cover the set Λ with a collection of subsets Ω_i where $|\Omega_i| \leq \delta$, called δ-cover set of Λ. If we now consider a parameter $s > 0$ we define the Hausdorff measure $H_\Lambda(\delta, s)$ of the set Λ:

$$H_\Lambda(\delta, s) = \inf\left\{\sum_{i=1}^{\infty} |\Omega_i|^s : \{\Omega_i\} \text{is a } \delta\text{-cover}\right\} \tag{2}$$

and the s-dimensional Hausdorff-Besicovitch measure $H_\Lambda(s)$ of Λ:

$$H_\Lambda(s) = \lim_{\delta \to 0} H_\Lambda(\delta, s). \tag{3}$$

The value of $H_\Lambda(s)$ jumps from ∞ to 0 for a certain value of the parameter s. The Hausdorff-Besicovitch dimension d_H is the critical value of s for which we have the discontinuity in H. Formally:

$$d_H = \sup\{s : H_\Lambda(s) = \infty\} = \inf\{s : H_\Lambda(s) = 0\}. \tag{4}$$

This concept of dimension does not provide a practical approach to measure the fractality of a set from experimental results. The difficulty is in essence due to the minimisation of the covering set, as discussed in TURNER (1998). For experimental purpose we apply a fractal dimension normally used to characterise fractals: such dimension is called *capacity dimension* d_C proposed by KOLMOGOROV (1958). The capacity dimension d_C of fractal objects such as those in Figures 2 - 7 is a measure of their space filling ability. For a set $\Lambda \epsilon R^n$ the capacity dimension is defined as follows:

$$d_C(\ell) = \lim_{\ell \to \infty} \frac{\ln N(\ell)}{\ln \ell}, \tag{5}$$

where $N(\ell)$ is the number of hyper-cubes (or n-dimensional cubes[4]) of size ε covering the fractal set Λ, and ℓ is the non-dimensional length $\ell = L/\varepsilon$. The value of ℓ corresponds to the number of units ε required to define the linear size L of the support. For example, if we consider a 2-D support as in Figures 2-7 and a pixel of size ε, the fractal dimensionality d_C of the fractal set (clusters) of Figure 2, at the third iteration, can be computed as follows:

$$d_C = \frac{\ln N(\ell)}{\ln \ell} = \frac{\ln 125}{\ln 27} = \frac{4.828...}{3.295...} = 1.464..., \tag{6}$$

Such fractal dimension has been used, for example, by KRANENBURG (1994) in the fractal characterisation of mud flocs and by WINTERWERP (1999) in the framework of Lagrangian modelling of mono-floc size time evolution.

---

[4]Hyper-cube is a generalised term in a n-dimensional space. When $n = 2$ we prefer to use the term box, since in our context we deal with objects embedded in 2-D supports.

This approach for computing the fractal dimensionality d_C can be performed by means of a technique called *box counting* which is widely discussed, for example, in ARGYRIS ET AL. (1994) and in TURNER (1998).

A different (probabilitstic) fractal dimension is the *information dimension* d_I, proposed by BALATONI AND RENYI (1957) as follows:

$$d_I(\ell) = \lim_{\ell \to \infty} \frac{I(\ell)}{\ln \ell}, \tag{7}$$

with $I(\ell)$ the Shannon information function, SHANNON (1948), defined as:

$$I(\ell) = -K \sum_{i=1}^{N} p_i \ln p_i, \tag{8}$$

where K is a constant and p_i is the probability that the i-th box of size ε is occupied by the fractal. The information function $I(\ell)$ represents a measure of the possible number of realisations that the system can have. Imagine to have an ordered set of n numbers $\{x_1, x_2, ..., x_n\}$ where all the x_i are equal to a constant value c. Imagine now to select $n^* \leq n$ adjacent numbers; the number of possible realisations n_p of the system is unique because all the $n - n^* + 1$ subsets show the same sequence, i.e. there is only one pattern in the system, $n_p = 1$. In this case, the information gain I is zero because the probability $p_j = 1 \forall$ $(n - n^* + 1)$. If the set of numbers $\{x_1, x_2, ..., x_n\}$ is composed of random values we can have a number of different patterns $n_p \geq 1$. n_p corresponds to the number of possible realisations. In such a case the information gain I is greater then zero.

A further fractal dimension is the *correlation dimension* d_K defined by GRASSBERGER AND PROCACCIA (1983). It can be formally written as follows:

$$d_K(r) = \lim_{r \to 0} \frac{\ln C(r)}{\ln r}, \tag{9}$$

where $C(r)$ is the correlation function between any two points $\mathbf{p}_i$ and $\mathbf{p}_j$ of the fractal:

$$C(r) = \frac{1}{N^2} \sum_{j=1}^{N} \sum_{i=j+1}^{N} H(r - |\mathbf{p}_i - \mathbf{p}_j|), \tag{10}$$

with H the Heaviside function, which is $H(x) = 0$ for $x \leq 0$ and $H(x) = 1$ for $x > 0$. The function $C(r)$ expresses the spatial correlation of two generic points $\mathbf{p}_i$ and $\mathbf{p}_j$ and is called the *correlation integral* of the fractal, while the parameter r is a critical Euclidian distance used to correlate two generic points with distance $|\mathbf{p}_i - \mathbf{p}_j|$.

2.3 Generalised dimensionality and multifractality

The definitions of fractal dimensions reported in the previous section have been investigated in detail by HENTSCHEL AND PROCACCIA (1983), leading to the concept of *fractal dimensionalities* (rather than fractal dimensions) and *multifractality*. The authors showed that an infinite number of generalised dimensions d_q is required to describe the characteristics of a fractal with an arbitrary inhomogeneous mass-density distribution, ARGYRIS ET AL. (1994). Let us once again consider a covering of a fractal by N boxes of size ε in a support of size L, such that $\ell = L/\varepsilon$; if N_i is the number of measuring points in the i-th box, then $p_i = N_i/N$ determines the probability of a measuring point lying in the i-th box. By using a mean information function I_q of order q-th, RENYI AND BALATONI (1957), as follows:

11

$$I_q(\ell) = -\frac{1}{1-q} \ln \sum_{i=1}^{N} (p_i)^q, \tag{11}$$

we write the generalised dimensionality of the q-th order as follows:

$$d_q(\ell) = \lim_{\ell \to \infty} \frac{I_q(\ell)}{\ln \ell} = -\frac{1}{1-q} \lim_{\ell \to \infty} \frac{\ln \sum_{i=1}^{N} (p_i)^q}{\ln \ell}. \tag{12}$$

GRASSBERGER AND PROCACCIA (1983) proved analytically that the fractal dimension-ions d_I, d_C and d_K are special cases of the generalised dimensionality d_q. In particular:

$$\begin{aligned} d_{q=0} &= d_C & \text{capacity dimension} \\ d_{q=1} &= d_I & \text{information dimension} \\ d_{q=2} &= d_K & \text{correlation dimension} \end{aligned} \tag{13}$$

The fractal dimensions are organised over a scale which can be written in the following form:

$$d_K \leq d_I = d_{q=1} \leq d_H \leq d_C = d_{q=0} \leq d_E,$$

$$d_q|_{\forall q \in \aleph} \leq d_E, \tag{14}$$

where the Euclidian dimension d_E is an integer number.

The concept of generalised fractal dimensionality expresses that fractals may show a spectrum of fractal dimensions as a function of the moment q. The presence of an infinite number of fractal dimensions can be associated with the presence of an infinite number of fractals, each with a different fractal dimension. This has been investigated in some fields of science and has resulted in the formulation of the *multifractal theory*. This approach to the fractal geometry states that some fractals are *multifractals*, that means that some fractals can be described as a combination of many *monofractals*. In particular, it can be proved that, for monofractals, the generalised dimension d_q collapses to a constant value $d_q = d_C$, that is the capacity dimension. In practice, for monofractals the following equality reads:

$$d_K = d_I = d_H = d_q|_{\forall q \in \aleph} = d_C \leq d_E \tag{15}$$

We can elaborate this concept by considering a homogeneous and a heterogeneous fractal set. In the first (monofractal) case, the generalised probability of a measure P scales with the length scale L as follows:

$$P \sim L^{d_f}, \tag{16}$$

where d_f is a fractal dimension. In the case of multifractals, the generalised probability within any i-th region P_i scales as:

$$P_i \sim L^{\alpha_i}, \tag{17}$$

with α_i the Lipschitz-Holder exponent or singularity strength. If we now imagine to cover a multifractal set with boxes of size ε and we define $N(\alpha)$ as the number of boxes where the probability P_i has singularity strength between α and $\alpha + d\alpha$, we achieve the following scaling law:

12

$$N(\alpha) \sim L^{-f(\alpha)}, \tag{18}$$

where $f(\alpha)$ is called the spectrum of fractal dimensions of the family of boxes with singularity α. $f(\alpha)$ is a continuous function of α and, usually, a unimodal curve with a maximum at $df(\alpha)/d\alpha = 0$. CHHABRA AND JENSEN (1989) proposed an efficient technique to compute the spectrum of fractal dimensionalities $f(\alpha)$ as discussed further in Section 4.

The concept of multifractality can be applied, for instance, to the description of the geometrical organisation of the primary particles forming a mud floc and to the growth probability distribution of fractal bodies. In Section 4 we apply this concept to some samples of real mud flocs and we give an interpretation of the results.

2.4 Thermodynamics of fractal sets

Fractal sets are complex structures characterised by fractal dimensionalities. The complexity of such structures has always been related to the predictability of the strange behaviours (chaotic, for instance) of the processes that, in nature, give form to fractal bodies. From this point of view, attempts have been made to look at the properties of fractals by using concepts of thermodynamics such as the one of *entropy*. A definition of the entropy S of a system, according to CHHABRA AND JENSEN (1989), is:

$$S = -\sum_i p_i \ln p_i, \tag{19}$$

where p_i is the probability to find a given pattern in the system. The state variable S corresponds to the Shannon information function I of Eq. 8, except for the constant K. Therefore, sometimes, it is also referred to as Shannon entropy. This definition of entropy (or, better, the information function I) is the information gain per single measurement, ARGYRIS ET AL. (1994)[5]. From a theorem by BILLINGSLEY (1965), the entropy S relates to the Hausdorff dimension d_H as follows[6]:

$$d_H = -\lim_{N \to \infty} \frac{\sum_{i=1}^{N} p_i \ln p_i}{\ln N} = \lim_{N \to \infty} \frac{S}{\ln N}. \tag{20}$$

The entropy of a fractal body is a measure of the disorder of its structure. Since S is a probabilistic-based quantity, it gives a measure of the probability to find recursive patterns at different scales of the set. Consequently, it measures the production of information for infinitesimal refinements in the estimation of the fractal dimension of the set. As already mentioned, the term information refers to the knowledge of the possible realisations of a system. For example, chaotic systems never repeat themselves identically and the information gain is much higher than the information of a system which shows repetitions. The information gain corresponding to one single realisation is zero, in fact $p_{\forall i} = 1$ and $I = 0$. Consequently, through Eq. 19 we obtain $S = 0$, which means that the system under investigation possesses the maximum order possible or, in analogy, the minimum uncertainty or the minimum complexity. In practice, complex structures can show regularities which are repeated in a (fully or nearly fully) self-similar way. The value of S expresses how much determinism (or

---

[5]If the measurement applies to a dynamical system we then find the definition of entropy due to Kolmogorov (1958) and Sinai (1959), also called KS-entropy: $H = \lim_{n \to \infty} \frac{\overline{I}(X^{(n)})}{n\Delta t}$, where X is the intersection of the partition of the support and the image measured at time t and $t + \Delta t$.

[6]In reality, it is more correct to refer to the information dimension rather than the Hausdorff dimension.

order) there is in such structures. From here derives the importance to evaluate the entropy S of real fractal structures (like mud flocs), in order to obtain a quantitative measure of the organisation or complexity of their mass distribution. We will develop this concept further in Section 5.1.

3 Numerical method for computing the fractal (capacity) dimension

We now discuss some items related to the numerical computation of the quantities previously introduced, paying attention to some details which are sometimes neglected.

3.1 Specification on the non-dimensional length ℓ

The technique normally employed for computing the fractal (capacity) dimension $d_f = d_C$ is called "box counting". It consists of making a series of partitions of the support (space domain) using boxes of decreasing sizes ε and plotting on a log-log scale the points of coordinates $(\ln N(\ell), \ln(\ell))$, with $\ell = L/\varepsilon$. Then, d_C is the slope of the linear regression of the points in the scatter plot, TURNER ET AL. (1998). This technique is based on the fact that the space domain is discrete and regular (square) and that the fractal develops itself over the whole domain in such a way that the length scale L is unique, VICSEK (1992). In the study of random cluster formation by numerical simulations as DLA (Diffusion Limited Aggregation) or CCA (Cluster Cluster Aggregation), it is common to use discrete and fixed lattice domains in which a fractal body grows. In these cases, it is not possible to identify a unique characteristic length of the cluster because the cluster itself grows randomly in an infinity number of directions. Moreover, natural fractals formed by aggregation, like mud flocs, do not grow on a discrete and regular frame. This is a strong difference between deterministic and real fractals. In the first case the length L is the frame size, while for growing fractals, the length L is not clearly defined and, consequently neither is ℓ.

For measuring purpose, therefore, different definitions of non-dimensional length ℓ have been proposed. Such definitions may be required when, for example, we want to characterise the hydrodynamic behaviour of an aggregate in a fluid medium. In this case it is possible to refer to the hydraulic radius R_{hyd} of a cluster (definition below, Eq25) such that the non-dimensional length ℓ reads as $\ell = R_{hyd}/R_p$, where R_p is radius of the primary particle. From this, a wide spectrum of possibilities is derived in order to identify a characteristic length L (diameter-like) of a complex cluster (real or artificial), through which a non-dimensional length ℓ and the fractal dimension d_C are computed.

3.2 Cluster diameter

Before defining the diameter of a cluster, it is not trivial that we approximate complex shapes by means of circles (in a 2-D domain) or spheres (in a 3-D domain). This approximation enables us to use a unique length scale easily accessible, such as the diameter. In nature, unfortunately, regular shapes are not often recognisable (as far as mud flocs, for instance, are concerned) and this leads to geometrical approximations.

We can then observe that regular shapes (spheres, cubes, etc.) possess a unique length scale, the so-called diameter. For a different set of shapes (cylinders, cones, etc.) the length scale is in general a compromise. For random fractal objects, the identification of a length scale remains rather fuzzy, see Table 1.

For this reason, many definitions can be used to quantify the diameter of a complex shape or cluster. Consider a 2-D support, discretised with boxes of the size of pixels, a number of definitions are plausible, such as:

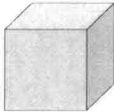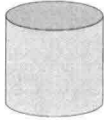1. *radius of gyration R_{gyr}*; it is defined as follows:

Object	Shape	Fractal Dimension	Length scale
	Sphere	$D_f = 3$	Unique
	Cube	$D_f = 3$	Unique
	Cylinder	$D_f = 3$	Compromise
	3D-Random Fractal	$2 < D_f < 3$	Fuzzy

Table 1: *Qualitative uncertainty relation between shape and linear length.*

$$R_{gyr} = \sqrt{\frac{1}{N}\sum_{i=1}^{N}|\mathbf{p}_i - \mathbf{p}_B|^2}, \tag{21}$$

where $|\mathbf{p}_i - \mathbf{p}_B|$ is the distance of the i-th box $\mathbf{p}_i$ from the center-of-mass $\mathbf{p}_B$ of the cluster.

2. *maximum radius* R_{max}; it is the maximum distance between the center of mass and any of the boxes of the perimeter. It is defined as follows:

$$R_{max} = \max\{|\mathbf{p}_i - \mathbf{p}_B|\}. \tag{22}$$

3. *minimum radius* R_{min}; it is the minimum distance between the center of mass and any of the boxes of the perimeter. It is defined as follows:

$$R_{min} = \min\{|\mathbf{p}_i - \mathbf{p}_B|\}. \tag{23}$$

4. *average radius* R_{ave}; it is the aritmetic mean of R_{max} and R_{min}

$$R_{ave} = (R_{max} + R_{min})/2. \tag{24}$$

5. *hydraulic radius* (areal equivalent radius) R_{hyd}; it is the diameter of a circle, whose area A is equivalent to the cluster's area:

$$R_{hyd} = \sqrt{\frac{A}{\pi}} \tag{25}$$

16

6. *perimeter equivalent radius* R_{per}; it is the diameter of a circle, whose perimeter P is equivalent to the cluster's perimeter:

$$R_{per} = \frac{P}{2\pi} \tag{26}$$

7. *major axis radius* R_{maj}; it is half of the maximum distance of any two boxes i and j belonging to the cluster.

$$R_{maj} = 0.5 \cdot max\{|\mathbf{p}_i - \mathbf{p}_j|\} \tag{27}$$

8. *box radius* R_{box}, it is half size of the minimum square circumscribing the object.

9. Feret radius R_{fer}; it is half distance s between two tangents on opposite sides of the cluster. It can be an average of nf repetition of the procedure from different directions:

$$R_{fer} = \frac{1}{nf} \sum_{i=1}^{nf} s_{nf} \tag{28}$$

Since the definition of Feret radius involves an arbitrary selection of directions, we prefer to take into account the definitions $1 - 8$ only.

3.3   Computation of d_C of random clusters

It is clear that each of the previous definitions of cluster radius R_x results in a different value of the non-dimensional length ℓ of the cluster, $\ell = \frac{R_x}{R_p}$. This causes the fractal dimension to change according to the definition of diameter employed, in fact:

$$d_C(R_x) = \frac{\ln N}{\ln\left(\frac{R_x}{R_p}\right)}. \tag{29}$$

The fractal dimension computed by means of the box radius R_{box} corresponds to the box counting technique employed in the original definition of fractal dimension of Eq. 5. In fact, the space domain relative to R_{box} corresponds to the minimum square support enveloping the fractal by a unique length scale $L = 2R_{box}$. For this reason, the fractal dimension $d_f(R_{box}) = d_C$ is the reference for validating the usage of other lengths than R_{box}.

We now perform some simple tests by evaluating the fractal dimension of some idealised fractals by using the measures of the cluster diameter introduced in Section 3.2. The aim is to validate the use of a numerical technique for fractal characterisation of both natural complex clusters (flocs) formed by turbulence-induced flocculation, and simulated clusters in the CCA regime as well. The test allows a comparison between the fractal dimension $d_C(R_{box})$ of Eq. 5 and the fractal dimensions $d_C(R_x)$ computed by means of the lengths R_x previously mentioned. In particular, we have identified two methods to compute the fractal dimensions. The first takes into account all the activated boxes of the fractal (pixels in our case, that correspond to the primary particles), while the second takes into account only the boxes activated within the radius R_x considered. Formally:

$$d_C^{(a)}(R_x) = \frac{\ln N^{(a)}}{\ln\left(\frac{R_x}{R_p}\right)}, \tag{30}$$

17

where $N^{(a)}$ is the total number of seeds forming the fractal. The second method reads as follows:

$$d_C^{(b)}(R_x) = \frac{\ln N^{(b)}}{\ln\left(\frac{R_x}{R_p}\right)}, \tag{31}$$

where $N^{(b)}$ is the number of particles whose distance $|\mathbf{p} - \mathbf{p}_B|$ from the center-of-mass $\mathbf{p}_B$ is smaller than R_x. The condition $|\mathbf{p} - \mathbf{p}_B| \leq R_x$ means that $N^{(b)} \leq N^{(a)}$ as well, and therefore we can already state that $d_C^{(b)}(R_x) \leq d_C^{(a)}(R_x)$.

3.4 Validation set

We introduce in Figure 8 the set of fractals which has been considered for testing the different measures of the non-dimensional length $\ell = R_x/R_p$ and the fractal dimension $d_C(R_x)$. All the fractals employed are built in a square frame of 300 by 300 pixels, except the fractal $F3$, whose size is 243 by 243 pixels because it is obtained by five multiplicative iterations of a 3 pixels-based initial element. The fractals $F1$ and $F2$ correspond to objects of known fractal (capacity) dimension, $d_C^{(F1)}(R_{box}) = 2$ and $d_C^{(F2)}(R_{box}) = 1$, respectively. $F3$ and $F4$ are artificial fractals while $F5$ and $F6$ are natural fractals from experimental measurements on kaolinite flocs. They have been obtained from pictures made by an analog camera of a resolution of 640 x 480 pixels, rotated in order to fit the minimum square support and resized to 300 x 300 pixels. The pixel is considered the unit quantity ε for the box counting technique. Black color means non activated pixel, white corresponds to activated pixel.

a) F1   b) F2   c) F3

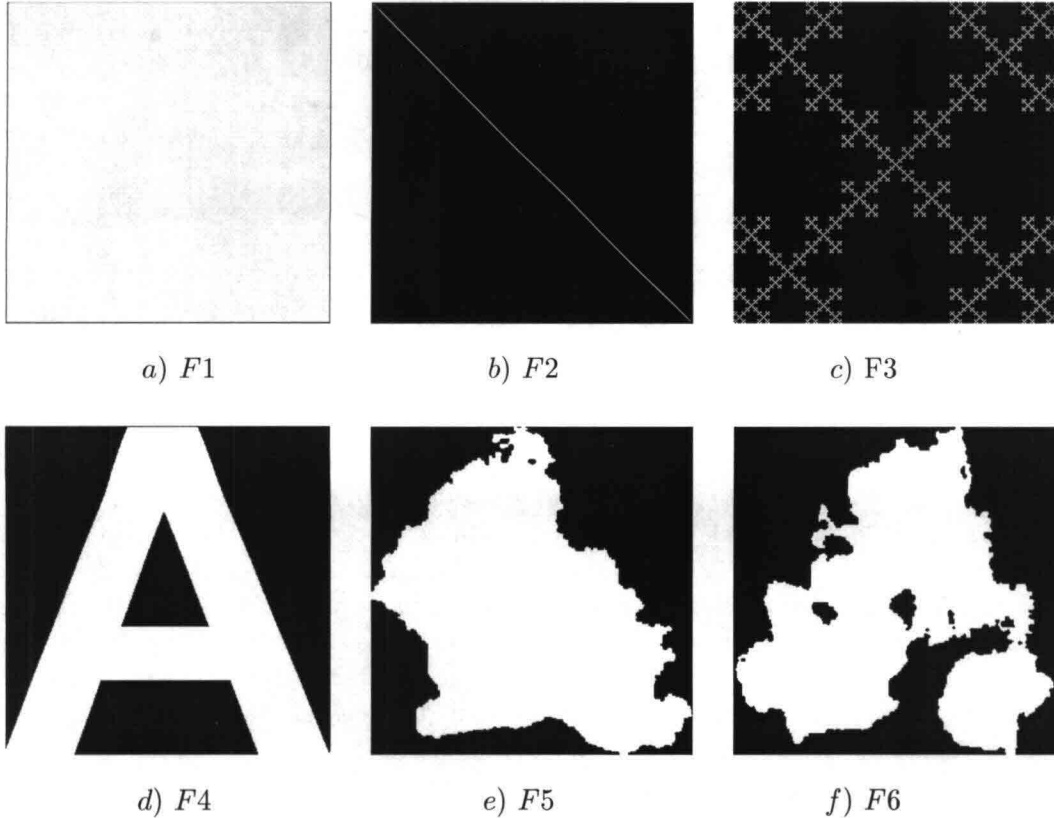d) F4   e) F5   f) F6

Figure 8: *Fractals used in the tests.*

3.5 Evaluation of the approach

The results of the computation from both methods of Eq. 30 and Eq. 31 are given in Table 2 a) and b) respectively.

As we can see from Table 2 a) a wide variability of fractal dimension is obtained when considering different lengths $L = 2R_x$. We cannot consider the computations of $d_C^{(a)}(R_x)$ (the first method) satisfactory since the measurements performed on the testing fractals show a strong over- or under- estimation. Indeed, 31% of the measurements fall either out of the upper limit $\overline{d_C} = 2$ or the lower limit $\underline{d_C} = 1$.

Things change when computing $d_C^{(b)}(R_x)$ (second method), that is considering only the seeds within the radius R_x, see Table 2 b). In this case the statistics show a strong convergence to the reference fractal dimension $d_C(R_{box})$, although some exceptions remain. By computing $d_C^{(b)}(R_x)$ only 17% of the measurements fall above or below the limits of the fractal dimension in a $2 - D$ domain. Moreover, all these cases involve fractal $F2$, which is a limit case of fractal dimension $d_C^{(F2)}(R_{box}) = 1$.

Let us now consider the results from the second computation. We can count the frequency $f(d_C^{(b)}(R_x) \simeq d_C(R_{box}))$ of occurrence of the dimension $d_C^{(b)}(R_x)$ nearest to the reference fractal dimension $d_C(R_{box})$ for all the fractals tested. In this way we can identify the corresponding length $L = 2R_x$ which properly approximates the fractal dimension $d_C(R_{box})$, as reported in Table 2 b). The result is that both R_{maj} and R_{hyd} occur as best approximations. We can identify R_{hyd} as a general length for the computation of the fractal dimension by considering its distance from the reference fractal dimension $d_C(R_{box})$, as reported in Table 3.

3.6 Considerations

A first set of results can be summarised:

1. The capacity dimension computed according to the definition of Eq. 5 represents a reference point for numerical investigations of fractal structures whatever their properties are. This definition makes use of a non-dimensional length $\ell = 2R_{box}$, which corresponds to the size of the minimum square enveloping the fractal.

2. Other lengths can be used for the computation of the fractal dimension. In particular we have evaluated two methods for the estimation of the capacity dimension d_C. The first takes into account all the seeds of the fractal, the second takes into account only the seeds within the length scale L chosen for the computation. Using the latter, the capacity dimension computed as a function of the hydraulic radius R_{hyd} in the corresponding partition of the support (second method, $d_C^{(b)}(R_{hyd})$) gives results very close to the reference fractal dimension $d_C(R_{box})$.

3. A convenient manner to compute the fractal dimension of growing bodies in numerical simulations like DLA or CCA, is the use of the hydraulic radius R_{hyd} as dimensional length of the cluster. This is much less time consuming than finding the minimum square circumscribing the fractal and applying the common algorithms.

a) Fractal dimensions $d_C^{(a)}$ (first method) from different lengths L.

Fractal F1 d_C	Radius [pixel]		Fractal F2 d_C	Radius [pixel]		Fractal F3 d_C	Radius [pixel]	
2.07	R_{gyr}	122	0.00	R_{min}	0	0.00	R_{min}	0
2.00	R_{min}	150	1.85	R_{hyd}	11	1.89	R_{hyd}	35
2.00	**R_{box}**	**150**	1.25	R_{per}	47	1.56	R_{ave}	86
1.96	R_{hyd}	169	1.07	R_{ave}	105	1.50	R_{gyr}	109
1.94	R_{ave}	180	1.04	R_{gyr}	121	**1.46**	**R_{box}**	**122**
1.92	R_{per}	190	**1.00**	**R_{box}**	**150**	1.38	R_{max}	171
1.89	R_{max}	211	0.94	R_{max}	209	1.38	R_{maj}	171
1.89	R_{maj}	211	0.94	R_{maj}	209	1.17	R_{per}	497

Fractal F4 d_C	Radius [pixel]		Fractal F5 d_C	Radius [pixel]		Fractal F6 d_C	Radius [pixel]	
2.18	R_{min}	65	2.16	R_{min}	75	2.65	R_{min}	29
1.98	R_{gyr}	106	2.05	R_{gyr}	97	2.03	R_{gyr}	100
1.96	R_{hyd}	114	1.96	R_{hyd}	126	2.02	R_{ave}	102
1.90	R_{ave}	134	1.95	R_{ave}	129	1.96	R_{hyd}	121
1.86	**R_{box}**	**150**	**1.90**	**R_{box}**	**150**	**1.88**	**R_{box}**	**150**
1.81	R_{maj}	176	1.87	R_{maj}	164	1.85	R_{maj}	163
1.77	R_{max}	202	1.83	R_{max}	183	1.83	R_{max}	176
1.75	R_{per}	212	1.73	R_{per}	258	1.64	R_{per}	343

a) Fractal dimensions $d_C^{(a)}$ (first method) from different lengths L.

Fractal F1 d_C	Radius [pixel]		Fractal F2 d_C	Radius [pixel]		Fractal F3 d_C	Radius [pixel]	
2.00	**R_{box}**	**150**	**1.00**	**R_{box}**	**150**	1.89	R_{gyr}	106
1.96	R_{min}	150	0.94	R_{max}	209	1.88	R_{hyd}	114
1.96	R_{gyr}	122	0.94	R_{maj}	209	1.88	R_{min}	65
1.94	R_{hyd}	169	0.94	R_{gyr}	121	**1.86**	**R_{box}**	**150**
1.93	R_{ave}	180	0.94	R_{ave}	105	1.85	R_{ave}	134
1.92	R_{per}	190	0.92	R_{per}	47	1.81	R_{maj}	176
1.89	R_{maj}	211	0.88	R_{hyd}	11	1.77	R_{max}	202
1.89	R_{max}	211	0.00	R_{min}	0	1.75	R_{per}	212

Fractal F4 d_C	Radius [pixel]		Fractal F5 d_C	Radius [pixel]		Fractal F6 d_C	Radius [pixel]	
1.93	R_{min}	15	1.95	R_{gyr}	97	1.91	R_{gyr}	100
1.91	R_{gyr}	101	1.95	R_{min}	75	1.91	R_{ave}	102
1.91	R_{ave}	106	1.92	R_{hyd}	126	1.90	R_{hyd}	121
1.90	R_{hyd}	123	1.92	R_{ave}	129	1.88	R_{min}	29
1.89	**R_{box}**	**150**	**1.90**	**R_{box}**	**150**	**1.88**	**R_{box}**	**150**
1.83	R_{maj}	178	1.86	R_{maj}	164	1.85	R_{maj}	163
1.80	R_{max}	197	1.83	R_{max}	183	1.83	R_{max}	176
1.60	R_{per}	415	1.73	R_{per}	258	1.64	R_{per}	343

a) Fractal dimensions $d_C^{(b)}$ (second method) from different lengths L.

Table 2: Fractal dimensions $d_C^{(a)}$ and $d_C^{(b)}$ computed from different lengths L.

$d_C(R_x)$ computed from	Frequency	$\lvert d_C(R_x) - d_C(R_{box}) \rvert$
R_{maj}	4	0.19
R_{hyd}	4	0.07
R_{ave}	3	-
R_{min}	3	-
R_{gyr}	2	-
R_{max}	1	-
R_{per}	0	-

Table 3: *Next nearest neighbours.*

4 Multifractal analysis of complex clusters

In this section we describe the calculation of the spectrum of fractal dimensionalities of the set of testing fractals shown in Figure 8. The aim it to extract information on the mass distribution and the growth probability distribution within complex structures.

4.1 Numerical computation of the multifractal spectrum $f(\alpha)$

We now apply the computation of the spectrum of fractal dimensionalities on the basis of the theory reported in Section 2.3. We have introduced the generalised fractal dimensionality in Eq. 12 and the scaling laws of multifractals in Eq. 18. The computation of the multifractal spectrum $f(\alpha)$ of Eq. 18, which corresponds to the fractal dimensionalities d_q of Eq. 12, requires the application of the Legendre transformation of a partition function. In many cases, the use of the Legendre transformation may give numerical problems and CHHABRA AND JENSEN (1989) proposed a direct method to evaluate the spectrum which reduces the computational efforts and preserves the reliability of the results. Operationally, we cover a set Λ in a support of size L with N boxes of size ε, we count the occupied area $M_i(\varepsilon)$ within each i-th box (in practice, the number of activated pixels) and we derive a probability $p_i(\varepsilon)$ as follows:

$$p_i(\varepsilon) = \frac{M_i(\varepsilon)}{\varepsilon^2}. \tag{32}$$

We now build a one-parameter family of normalised measures $\mu(q, \varepsilon)$:

$$\mu_i(q, \varepsilon) = \frac{p_i(\varepsilon)^q}{\sum p_i(\varepsilon)^q}, \tag{33}$$

such that $\sum_i \mu_i(q, \varepsilon) = 1$. The exponent q represents a weight moment which gives relevance to more singular regions[7] if $q > 1$, it accentuates the less singular regions if $q < 1$, and it replicates the original measure if $q = 1$. Now, the fractal dimensionality $f(q, \varepsilon)$ is given by:

$$f(q, \varepsilon) = - \lim_{N \to \infty} \frac{\sum_{i=1}^{N} \mu_i(q, \varepsilon) \cdot \ln \mu_i(q, \varepsilon)}{\ln N} = \lim_{\varepsilon \to 0} \frac{\sum_{i=1}^{N} \mu_i(q, \varepsilon) \cdot \ln \mu_i(q, \varepsilon)}{\ln \varepsilon}, \tag{34}$$

where $N = (L/\varepsilon)^2$ is the number of boxes. In addition, we can compute the average value of the singularity strength α_i by evaluating:

$$\alpha(q, \varepsilon) = - \lim_{N \to \infty} \frac{\sum_{i=1}^{N} \mu_i(q, \varepsilon) \cdot \ln p_i(q, \varepsilon)}{\ln N} = \lim_{\varepsilon \to 0} \frac{\sum_{i=1}^{N} \mu_i(q, \varepsilon) \cdot \ln p_i(q, \varepsilon)}{\ln \varepsilon} \tag{35}$$

Eq. 34 and Eq. 35 provide a relationship between the fractal dimensionality f and an average singularity strength α as functions of the parameter q; f is, in fact, $f(\alpha(q))$, CHHABRA AND JENSEN (1989). By means of this relation we attain an efficient method to compute the spectrum of fractal dimensionalities formally introduced with Eq. 12.

The dimensionality spectrum of the testing fractals of Figure 8 has been computed for values of q ranging within $q = \{-20, ..., 20\}$ and for $\varepsilon = 100$ pixels. The results are shown in Figures 9, 10, 11 and 12. In particular, Figure 9 and 10 show the spectrum of the fractals under investigation as a function of the moment q and the singularity strength α respectively. We can observe that the fractals $F1$, $F2$ and $F3$ have a constant value of f, Figure 9. In

---

[7] A region of the fractal has high singularity strength when it is densely occupied by the fractal, and low singularity strength when it is weakly occupied by the fractal.

practice, the fractal dimensionality d_q collapses into a unique value, corresponding to a unique value of the singularity strength α, Figure 10. This is evidence of the fact that F1, $F2$ and $F3$ are monofractals.

The fractals $F4$, $F5$ and $F6$ show a curved spectrum representing the fractal dimensions within the set. The function $\alpha(q)$, singularity strength, is drawn in Figure 11 as a function of q, where $F1$, $F2$ and $F3$ again show that the distribution of singularity strength is invariant with different moments q. The fact that F4, F5 and $F6$ show a range of singularities α means that each of the q-th $\mu(q, \varepsilon)$-partitions of the sets possesses a distinct fractal dimensionality. This is evidence of the multifractality nature of F4, $F5$ and F6.

The multifractal spectrum shows the region of probability of growth of a growing cluster. The growth process is dominated by those regions that have the largest growth rates of probabilities. The scaling properties of those parts correspond to small values of α or the "left side" of the spectum $f(\alpha)$, MEAKIN (1998). It is, in fact, in the regions of lowest presence of mass that the growth has the highest probability of occurrence.

The multifractal analysis is therefore a powerful tool to identify and characterise fractal structures. In the case of multifractals, such tool aids the modelling of scaling properties as size and porosity, and can be used to predict the probability distribution of dominant growing patterns of real flocs. The 2-D measurements of real mud flocs will be characterised by their multifractal spectrum in order to obtain the dominant scaling behaviours to be inserted in a population model and improve the predictive capability of floc size distribution and settling velocity in laboratory conditions.

4.2 Considerations

A set of considerations, based on the previous results, is summarised as follows:

1. We have seen that real fractal clusters (kaolinite aggregates) and part of artificial fractals have multifractal properties. This means that they are characterised by a full range of fractal dimensions (multifractal spectrum $f(\alpha)$). Multifractals are a combination of an infinite number of monofractals, with an overall multiscaling behaviour.

2. Real fractal flocs are statistically self-similar, as many studies in literature have already reported. This is physically observed also in the multifractal spectrum, which shows that complex real fractals are self-similar only at small ranges of length scales. From a theoretical point of view, this means that the density and porosity distributions do not scale with the same power law at different scales. Consequently, we can suppose that also the kinematic behaviour of floc aggregation and break-up change the scaling laws over different scales. Potentially, it is possible to improve the accuracy of predictive models of growth processes, like the Lagrangian formulation of floc size time evolution, WINTERWERP (1999), by considering dominant scaling laws (namely the fractal dimensionalities) for given ranges of length scales.

3. The multifractal spectrum can be used to study the distribution of the growth probabilities within a growing cluster. In particular, low values of the singularity strength $\alpha(q)$ are associated with the regions of the cluster that have the highest probability of growth, MEAKIN (1998). As a consenquence, the rates of growth of fractal flocs can be identified in space and modelled consequently in a 2-D domain.

4. The multifractal nature of particulate flocs might be evidence of the fact the real fractals grow, in nature, in a dynamic state far from equilibrium. A thermodynamic equilibrium
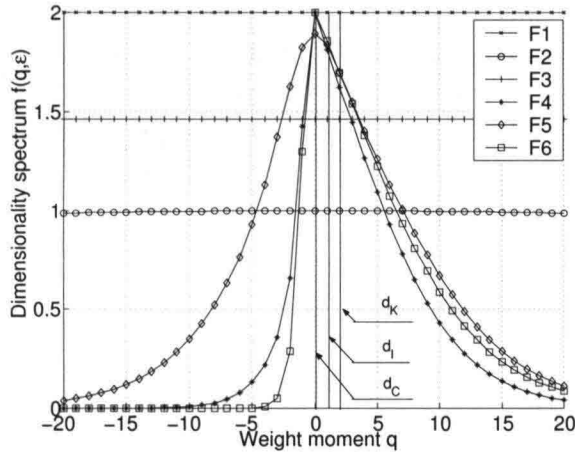
24

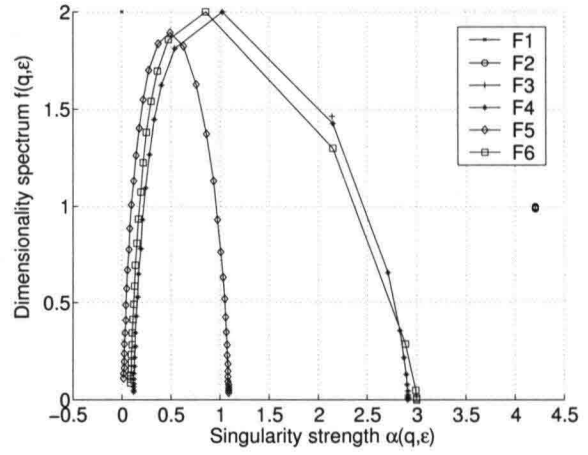Figure 9: *Dimensionality spectrum $f(q, \varepsilon)$ as a function of the moment q.*

Figure 10: *Dimensionality spectrum $f(q, \varepsilon)$ as a function of the singularity strength $\alpha(q, \epsilon)$.*
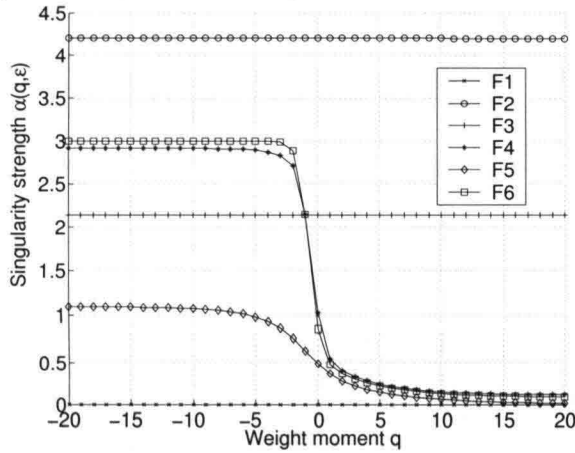

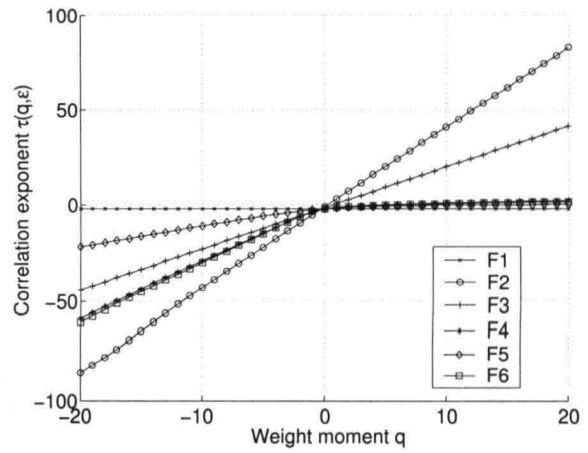Figure 11: *Correspondence between $\alpha(q, \epsilon)$ and q.*

Figure 12: *Scaling relation between $\tau(q, \epsilon)$ and q.*

has been observed in the field of crystal growth, while chemical reactions seem to occur with a non-equilibrium (far-from-equilibrium) behaviour, NICOLIS AND PRIGOGINE (1977). By analogy, we can imagine that also the growth process of cohesive particles in a turbulent field possesses non-equilibrium features. In this case, the multifractality properties of such particles, by being $f(\alpha)$ related the the entropy of the system, could be a measure of the distance from the equilibrium of the dynamics of those particles. In practice, the multifractality would be an evidence of distance from equilibrium.

5. The emergence of ordered patterns in dynamical systems far from equilibrium has been studied in detail by NICOLIS AND PRIGOGINE (1977) in chemistry and by MATURANA AND VARELA (1972) in biology. Their investigations converged to the theory of "self-organisation" or "autopoiesis" by showing that systems far from equilibrium can be sources of negative entropy and consequent onset of spontaneous order. This results in the autonomous organisation of the system towards complex structures. Cohesive particles show such behaviour as well, and the basic idea that particulate cohesive systems follow an analogous behaviour of self-organisation can be stated here. The emergence of self-organisation within a system made by cohesive particles would result

25

in the emergence, for example, of dominant floc sizes in a population of floc different in size. Such phenomenon has been observed and measured in laboratory, VAN LEUSSEN (1984) and WINTERWERP (1999), and in situ DE BOER (2000). The self-organising properties of those systems can be the physical explanation of the fact that, in general, the floc size distribution of a population of flocs is organised in a bimodal curve.

6. We can distinguish a microscopic and a macroscopic level. At a microscopic level, fractal flocs evolve individually in a state far from equilibrium. At a macroscopic level, a population of fractal flocs approaches a statistically steady state equilibrium.

5 Thermodynamic organisation of fractal clusters

We now apply the concepts of entropy with the thermodynamic formalism introduced in Section 2.4.

5.1 Entropy of fractal clusters

The measure of how much determinism lies in a fractal system can be related to the entropy of the system itself. The entropy of a system is a state variable and gives an indication of its complexity because it is related to the probability to find recursive patterns in it. In practice, the higher the probability to match a given pattern the lower the entropy is. We can use this concept to characterise the mass organisation of a floc (that is the distribution of clay particles within a floc) according to the following procedure. We define a box size $\varepsilon < L$ to generate a partition of the floc support of size L. The number of boxes is then $N = (L/\varepsilon)^2$ and for each i-th box we compute the number of activated pixels (corresponding to the area) $M_i(\varepsilon)$. Now, in agreement with Eq. 19 from the histogram of the function $M_i(\varepsilon)$ we obtain the probability $p_i(\varepsilon)$ and the number of patterns $N_p \leq N$. By using $p_i(\varepsilon)$ in the definition of entropy S given by the Shannon theorem of Eq. 19, we attain the entropy $S(\varepsilon)$ as follows:

$$S(\varepsilon) = -\sum_{i=1}^{N_p} p_i(\varepsilon) \log\left[p_i(\varepsilon)\right]. \tag{36}$$

Results of the computation of S for the testing fractals are shown in Figure 13, for box sizes $\varepsilon = \{5, 10, 50, 100\}$ relative to $F1$, $F2$, F4, $F5$ and $F6$, and $\varepsilon = \{3, 9, 27, 81\}$ relative to $F3$. For small box sizes (say, $\varepsilon = 3$ and $\varepsilon = 5$) we obtain an interesting numerical characterisation of the fractals. The fractals $F1$ and $F2$ show very low values of entropy; the obvious explanation is that they both are not real fractals. The organisation of $F1$ and $F2$ is very high and essentially "Euclidian" in the meaning that they do not show fractalisation, since $d_C^{(F1)}(R_{box}) = 1$ and $d_C^{(F2)}(R_{box}) = 2$. We can also say that $F1$ and $F2$ have a very low level of complexity, in fact they do not show any sort of self-similarity. As already said in Section 2.2, the less the number of patterns found in a system, the lower the value of the state variable S. S is zero for the fractals $F1$ and $F2$, because there is only one pattern recognisable in the system[8].

The entropy $S^{(F3)}$ of the fractal $F3$ is much higher than $S^{(F1)}$ and $S^{(F2)}$. This is due to the fact that $F3$ is a classic deterministic and fully self-similar fractal with an internal organisation much more complex than the previous fractals. The entropy $S^{(F4)}$ is higher still. That means that the internal oganisation of $F4$ is complex. Although not self-similar, the fractal $F4$ in fact has a spatial mass distribution organised over a more complex structure than $F1$ and $F2$ [9].

The fractals $F5$ and $F6$ show entropy levels that are very high compared to all the previous fractals. This can be explained by the fact that they are stochastic clusters as well as stochastic are the processes which formed them by aggregation and break-up. The structural organisation is very complex with respect to the organisation of all the previous

---

[8]The fractal $F2$ shows values of S close to zero because of numerical approximations in the computation of S.

[9]The level of organisation of $F4$ can not be related in any way to the "semantic organisation" of the shape itself. The semantic meaning of $F4$ is something totally independent from what we want to pinpoint in this study.

fractals, because of the large number of patterns found in the partitioning procedure of the set.

The entropy S, beside the meaning of organisation, can also be interpreted as a measure of the predictability of the system. Since S is derived from the probability of recurrent patterns in an object, we can deduce the growth probability of a cluster with patterns that are already present in the structure. In particular cases (self-similar fractals) those patterns are already present in the structure, either at the same scale, or smaller. Moreover, fractal mud flocs are subject to a continuous-in-time process of restructuring due to aggregation and breakage; by computing the entropy level of a floc at different stages of its growth it is possible to identify different regimes of the flocculation mechanisms which are stored in the structure of the floc in the same way as a "memory" of the aggregation and break-up steps passed along the time. Potentially, it is possible to identify entropy variations within the floc structure that are caused by different dominant processes, like turbulent shear rate or differential settling. This technique would enable the identification of bifurcation behaviours in the evolution processes of growing flocs.

The state variable S, being related to the fractal dimension d_I, might be fundamental in characterising the determinism present in aggregation and break-up processes; the information achievable from this investigation can in fact aid the modelling of the physics beyond the flocculation processes of colloidal particulate systems in a turbulent environment.
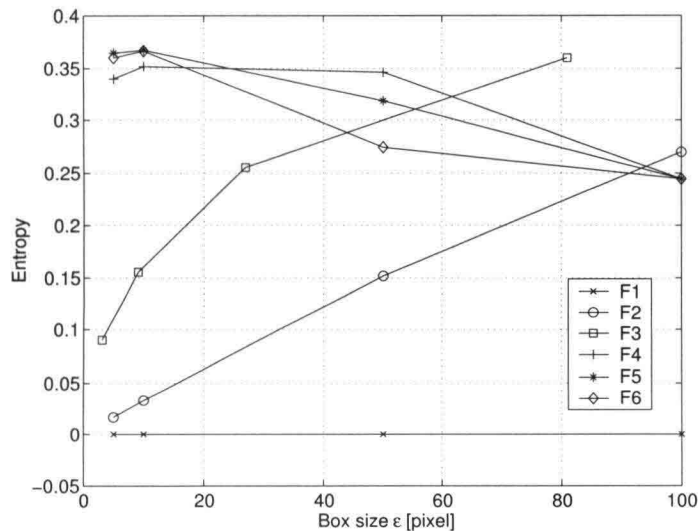

Figure 13: *Entropy.*

5.2 Approximate entropy Ψ of fractal clusters

The approximate entropy function Ψ is a state variable similar to S. It gives a measure of the organisation of a cluster and it is based on its mass distribution. It is computed by counting the number of the next nearest neighbours patterns[10] in a partition of the support in analogy to the one performed in the computation of S. Therefore, we set a box size ε and we compute the mass $M_i(\varepsilon)$ for each box and the corresponding probabilities $p_i(\varepsilon)$. Then we set a similarity parameter r usually based on the standard deviation of $p_i(\varepsilon)$ in the form

---

[10]In this approach, differently from the entropy, we look at similar patterns and not only at identical patterns.

$r = 0.1 \cdot std(p_i(\varepsilon))$ and we count the number $N_i(\varepsilon, r)$ of patterns $\{p_j(\varepsilon) : j \neq i\}$ with distance $|p_i - p_j| \leq r$. We define a first quantity $\Phi_i(\varepsilon, r)$ as follows:

$$\Phi_i(\varepsilon, r) = \frac{N_i(\varepsilon, r)}{(N - \varepsilon + 1)^2}. \tag{37}$$

We repeat the same procedure for $\varepsilon + 1$ in order to obtain the quantity $\Phi_i(\varepsilon + 1, r)$ as follows:

$$\Phi_i(\varepsilon + 1, r) = \frac{N_i(\varepsilon + 1, r)}{(N - \varepsilon)^2}. \tag{38}$$

The function $\Psi(\varepsilon, r)$ is eventually defined as follows, Pincus (1991):

$$\Psi = \frac{\sum_{i=1}^{(N-\varepsilon+1)^2} \ln \Phi_i(\varepsilon, r)}{(N - \varepsilon + 1)^2} - \frac{\sum_{i=1}^{(N-\varepsilon)^2} \ln \Phi_i(\varepsilon + 1, r)}{(N - \varepsilon)^2} \tag{39}$$

The results of the approximate entropy function Ψ for the testing fractals are shown in Figure 14, for $\varepsilon = \{5, 10, 50, 100, 150\}$. The results collected for the testing fractals confirm the results already obtained for the computatuion of the entropy S.
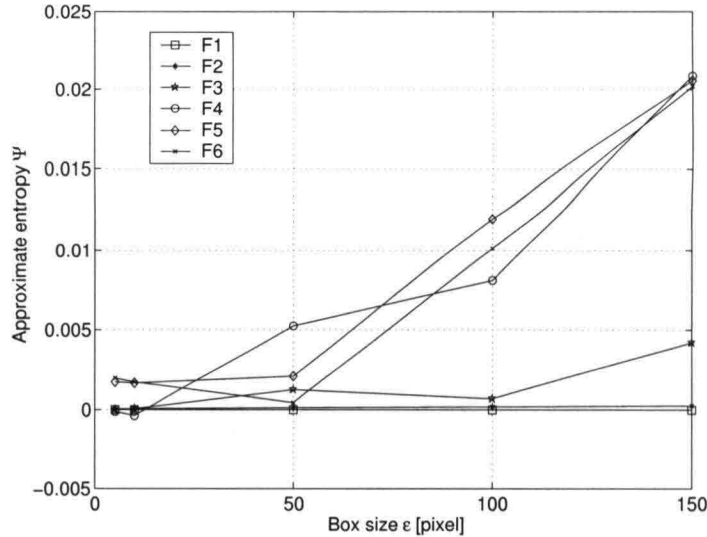

Figure 14: *Approximate entropy function Ψ.*

5.3   Considerations

We now state some considerations which are related to the considerations of Section 4.2, concerning the multifractal analysis of complex structures.

1. We have seen in the multifractal theory of Section 2.3 and in the entropy characterisation of Section 2.4 that fractal structures can be classified according to their complexity. The results of multifractal analysis and the computation of the state variable entropy S express that Euclidian structures do not have similarity properties. This generally corresponds to constant levels of entropy S at different length scales. Moreover, the values of entropy S are generally very low.

29

2. Monofractal structures have a fully self-similar organisation of the mass distribution. In this case, the level of entropy is generally higher than in Euclidian structures and it has a constant-like slope in a log-log scale representation. This corresponds to higher level of complexity compared to Euclidian structures.

3. Multifractal structures are statistically self-similar and have a full range of fractal dimensionalities. This results in mass distributions of a higher level of complexity. In such a case, S can show very high values, but we cannot say what trend S has at different scales.

4. The state variable entropy S and the approximate entropy Ψ are a measure of the complexity of a structure. They give a measure of the probability to find recursive patterns. Therefore, S and Ψ measure the probability that a structure might evolve in a certain way rather than another. By induction, it gives also an idea of the quantity of randomness and determinism present in a structure.

5. The structure of a multifractal possesses a sort of memory of the growth dynamics that formed it. The evolution of the entropy at different stages of the growth can, therefore, detect bifurcation behaviours in the growth process. Fractal mud flocs can show different levels of entropy as a consequence of different growth mechanisms, such as those of turbulence shear rate and differential settling.

6 Euclidian organisation of fractal clusters

6.1 Symmetry of fractal clusters

Growing fractal clusters may show properties of symmetry. The presence of symmetries in the structure of an aggregate may give indications of the mechanisms of formation. In particular, we can interpret a high level of symmetries as a consequence of high determinism in the system and a low level of symmetries as a sign of random (noisy) mechanisms. The presence of symmetries corresponds to redundant patterns, a property that can be detected by the state variable entropy as well.

A simple correlation function $\gamma(\theta)$ can be used to identify the symmetries within a fractal aggregate. The technique consists of doubling the image of a fractal, rotating the copy around the geometric center and measuring the overlapping area as a function of the angle θ. The normalised function $\gamma(\theta)$ can be written as follows:

$$\gamma(\theta) = \frac{\int_{(I_0 \cap I_\theta)} \mathbf{P}}{\int_{I_0} \mathbf{P}} = \frac{1}{N} \sum_{i=1}^{N} \{\mathbf{p}_i : \mathbf{p}_i \epsilon I_0 \cap I_\theta\}, \tag{40}$$

where I_0 is the reference image of the fractal, I_θ is the image of the fractal rotated by an angle θ and $\mathbf{p}_i$ is the vector position of the seeds, or pixels. The correlation function $\gamma(\theta)$ is $\gamma(\theta) = 1$ for $\theta = 0^o$ and $\theta = 360^o$ and it is symmetric with respect to $\theta = 180^o$.

The results of the computation of $\gamma(\theta)$ for the testing fractals are shown in Figure 15. For symmetric fractals like $F1$, $F2$ and $F3$ the function $\gamma(\theta)$ has clear peaks about 90°, 180° and 130° respectively. For complex clusters like $F4$, $F5$ and $F6$ no peaks are clearly distinguishable. In the cases of $F5$ and $F6$, the nearly white noise correlation might be evidence that the object under investigation has complex fractal properties and that those properties are due to a certain amount of determinism and randomness. The presence of clear peaks may be associated with deterministic or, at least, regular growths. $\gamma(\theta)$ can be used, coupled with the entropy S, to identify deterministic organisation in a growing cluster.
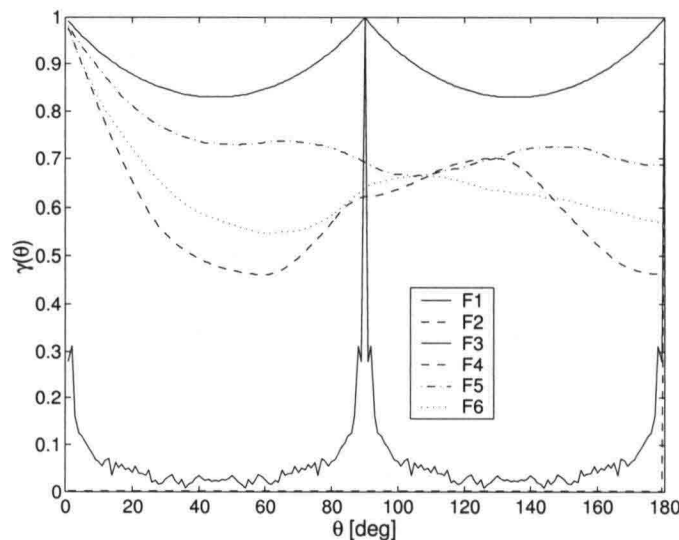

Figure 15: *Symmetry $\gamma(\theta)$ of the testing fractals.*

6.2 Eccentricity and shape factor of fractal clusters

A geometrical characterisation of complex fractal clusters such as mud flocs, is the measure of their eccentricity. We can imagine that complex kinematics may result in anisotropic pattern formation. This causes the cluster to grow (or decrease) with different rates along various directions. A measure of the static isotropy in the growth/decrease of floc size can therefore be achieved by evaluating the eccentricity of the shape by means of a shape factor f_e, here defined;

$$f_e = 1 - \frac{L_{min}}{L_{max}}, \qquad (41)$$

where L_{min} and L_{max} are the minimum and maximum sizes of the support enveloping the fractal. In this definition, L_{min} and L_{max} correspond to the minimum and maximum Feret diameters introduced in Eq. 28. The eccentricity factor f_e ranges in the interval $0 \leq f_e \leq 1$; values of f_e close to $f_e \simeq 1$ are indicative of high eccentricity, values of f_e close to $f_e \simeq 0$ mean regularity and symmetry in the peripherical distribution of the seeds, with a consequent low eccentricity.

A shape factor f_s of a cluster can be obtained from the eccentricity factor f_e itself. In particular, we can define a shape factor f_s as:

$$f_s = 1 - f_e = \frac{L_{min}}{L_{max}}. \qquad (42)$$

The factor f_s ranges as f_e in the interval $0 \leq f_s \leq 1$ but this time $f_s = 1$ means that the bulk of cluster is uniformly distributed around its center. Then f_e can be employed in modelling the settling of mud flocs, aggregation and break-up efficiency or other quantities which involve directly any impact of the shape of an aggregate in a given process.

We show in Figure 16 and in Figure 17 respectively the eccentricity and the shape factor of the fractals tested.
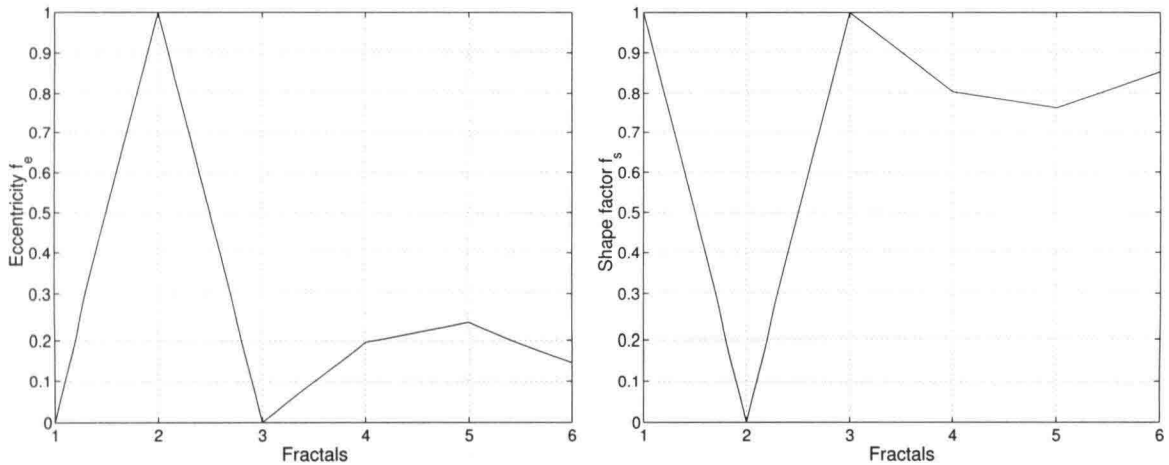

Figure 16: *Eccentricity f_e of the testing fractals.* Figure 17: *Shape factor f_s of the testing fractals.*

6.3 Porosity of fractal clusters

The porosity of a random fractal cluster can be evaluated by the ratio between empty and occupied regions within a given length. If we use the hydraulic radius R_{hyd}, the porosity e is

written as:

$$e = 1 - \frac{\int_I \{ \mathbf{p} : |\mathbf{p} - \mathbf{p}_b| \leq R_{hyd} \}}{\pi R_{hyd}^2} = 1 - \frac{\sum_{i=1}^N \{ \mathbf{p}_i : |\mathbf{p}_i - \mathbf{p}_B| \leq R_{hyd} \}}{\pi R_{hyd}^2}, \qquad (43)$$

where $|\mathbf{p}_i - \mathbf{b}_B|$ is the distance of the seed $\mathbf{p}_i$ from the center of mass $\mathbf{p}_B$. The results of the porosity e for the testing fractals are reported in Figure 18.

The porosity e and the quantities $\gamma(\theta)$ as defined in Eq. 40 are statistically correlated. In particular, the complement of the average value of $\gamma(\theta)$ approximates with good agreement the value of the porosity computed as in Eq. 43:

$$1 - \overline{\gamma(\theta)} = 1 - \frac{1}{\pi} \int_0^\pi \gamma(\theta) d\theta \simeq e. \qquad (44)$$

In fact, considering Eq. 40 and Eq. 43 we obtain the following relation:

$$1 - \frac{\int_I \{ \mathbf{p} : |\mathbf{p} - \mathbf{p}_b| \leq R_{hyd} \}}{\pi R_{hyd}^2} \simeq 1 - \frac{1}{\pi} \int_0^\pi \gamma(\theta) d\theta,$$

$$\frac{\int_I \{ \mathbf{p} : |\mathbf{p} - \mathbf{p}_b| \leq R_{hyd} \}}{\pi R_{hyd}^2} \simeq \frac{1}{\pi} \int_0^\pi \frac{\int_{(I_0 \cap I_\theta)} \mathbf{P}}{\int_{I_0} \mathbf{P}} d\theta = \frac{\frac{1}{\pi} \int_0^\pi \int_{(I_0 \cap I_\theta)} \mathbf{P} d\theta}{\int_{I_0} \mathbf{P}}.$$

Being πR_{hyd}^2 the area of the fractal by definition of Eq. 25, we obtain that:

$$\pi R_{hyd}^2 = \int_{I_0} \mathbf{P},$$

and consequently that:

$$\int_I \{ \mathbf{p} : |\mathbf{p} - \mathbf{p}_b| \leq R_{hyd} \} \simeq \frac{1}{\pi} \int_0^\pi \int_{(I_0 \cap I_\theta)} \mathbf{p} d\theta.$$

Numerical evidence of the relation of Eq. 44 is given in Figure 18.
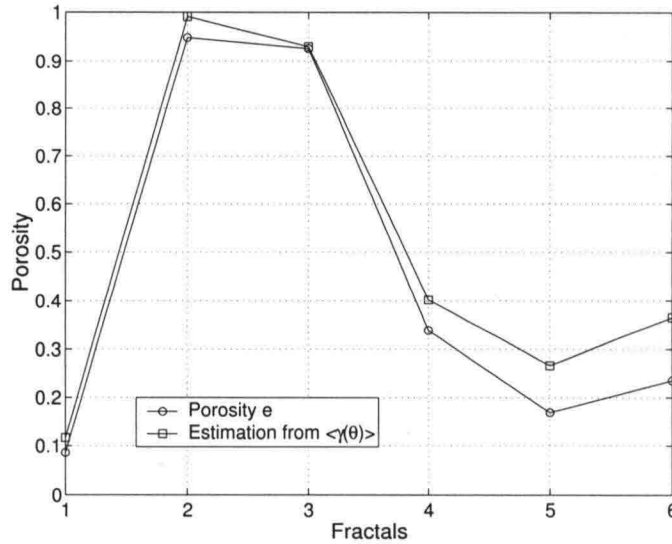

Figure 18: *Porosity e and $\overline{\gamma(\theta)}$.*

33

6.4 Considerations

We collect a set of considerations as follows.

1. From the analysis of the angular correlation function $\gamma(\theta)$ we have seen that complex structures (fully and statistically self-similar) have a noisy correlation. $\gamma(\theta)$ can be used to detect peaks of symmetry in complex shapes as fractal cluster.

2. The eccentricity factor f_e of a shape has been used already in modelling the growth and the settling processes of flocs made by cohesive particles, for example in Winterwerp (1999). The eccentricity factor and the shape factor are directly related to each other in the formulation of Eq. 41 and Eq. 42.

3. The porosity properties of fractal shapes can be measured by the angular correlation function $\gamma(\theta)$. The porosity is also related to the space filling ability of the object under study and therefore it is related to its fractal dimension.

7   Conclusion

In this section we summerise and discuss the most important issues highlighted within this survey.

We have established a hierarchical classification tree (Figure 1) of fractals on the basis of the large-scales properties that fractals show. Such tree takes into account artificial and real fractals. From those, a series of properties is derived in the form of cascade: deterministic and random, fully self-similar and statistically self-similar, fully homogeneous and statistically homogeneous, monofractal and multifractal clusters.

We have computed the capacity dimension of a set of testing fractals in order to indicate dimensional length scales different from the support size $L = 2R_{box}$. We have found that the hydraulic radius R_{hyd} can be used to compute the capacity dimension of any 2-D fractal with reliable accuracy. This allows a fast computation, above all for DLA and CCA simulations, as discussed already in Section 3.6

We have applied the multifractal approach to characterise the geometrical structure of fractals in general. This approach will be employed in the analysis of real measurements of kaolinite and mud flocs in laboratory conditions. The laboratory experiments will be performed in the settling column with temperature, concentration and turbulence controlled conditions. The multifractal analysis of the population of flocs at different stages of growth will highlight what the dominant behaviours (scaling laws) are within a set of flocculating aggregates. Operationally, a population of flocs can be grouped into classes of similar properties to calibrate the parameters of a multisize population equation. Such an approach would lead to an improvement in the understanding of the physics beyond the flocculation processes and the modelling capacities of the current equations.

We have applied a thermodynamic approach to study the complexity of fractal flocs by means of the state variable entropy. This is a fruitful interpretative tool to describe the organisation of primary particles in a complex set. We potentially believe that the entropy can have a relevant role in the modelling of growing flocs, although not directly in any population equation.

Finally, we have characterised complex flocs by means of the traditional Euclidian tools (shape factor, porosity and eccentricity). Those parameters have already been used in some formulations of floc size evolution and settling velocity. We will evaluate them also in our experiments in order to calibrate empirical parameters of a population equation.

35

List of Figures

List of Tables

37

References

[1] ARGYRIS J., FAUST G., HAASE M., 1994, *An exploration of chaos*, John Argyris F.R.S.

[2] BO H., FUSHENG Y., QINGYU T., TIN-CHEUNG C., 1998, *Approximate entropy and its preliminary application in the field of EEG and cognition*, Proceedings of the 20-th annual internation conference of the IEEE Engineering in Medicine and biology Society, Vol. 20, No. 4, 2091-2094.

[3] DE BOER D. H., STONE M., LÉVESQUE L. M. J., 2000, *Fractal dimensions of individual flocs and floc population in streams*, Hydrological Processes, No. 14, pp. 653-667.

[4] DYER K. R., 1989, *Sediment processes in estuaries: future research requirements*, Journal of Geophisical research Vol. 94(c10), No. 14, pp. 327-332.

[5] CHHABRA A., JENSEN R. V., 1989, *Direct determination of the $f(\alpha)$ singularity spectrum*, Vol. 62, No. 12, pp. 1327-1330.

[6] JENSEN M. H., KATANOFF L. P., PROCACCIA I., 1987, *Scaling structure and thermodynamics of strange sets*, Physical Review A, Vol. 56, No. 3, pp. 1409-1419.

[7] KRANENBURG C., 1994, *The fractal structure of cohesive sediment aggregates.*, Estuarine, Coastal and Shelf Science, No. 39, pp. 451-460.

[8] KRANENBURG C., 1998, *Effects of floc strength on viscosity and deposition of cohesive sediment suspensions*, Continental Shelf Research.

[9] GRASSBERGER P., PROCACCIA I., 1983, *Characterization of strange attractors*, Physical Review Letters, Vol. 50, No. 5, pp. 346-349.

[10] IKEDA K., DAIDO H., AKIMOTO O., 1980, *Optical turbulence: Chaotic Behavior of Transmitted Light from a Ring Cavity*, Physical Review Letters, Vol. 45, No. 9, pp. 709-712.

[11] MACH J., MAS F. AND SAGUES F., 1995, *Two representations in multifractal analysis*, Journal of Physics, Vol. 28, pp. 5607-5622.

[12] MAGGI F., *Flocculation of cohesive sediments: literature survey*, Report 1-02, Delft University of Technology.

[13] MATURANA H., R., VARELA F., J., 1972, *Autopoiesis and cognition*, Ed. Cohen R., S. and Wartofsky M., W., Dordrecht, Holland.

[14] MEAKIN P., 1998, *Fractals, Scaling and Growth Far From Equilibrium*, Cambridge University Press.

[15] PATHRIA R. K., 1978, *Statiatical Mechanics*, Pergamon Press.

[16] PINCUS S. M., 1991, *Approximate entropy as a measure of system complexity*, Proc. Natl. Acad. Sci. USA, Vol. 8, 222297-2301

[17] NICOLIS G., PRIGOGINE I., 1974, *Self-organisation in Non equilibrium systems*, Wiley J. and Sons Edit.

[18] TENNEKES H. AND LUMLEY J. L., 1973, *A first course in turbulence*, The MIT Press.

[19] TURNER M. J., BLACKLEDGE J. M. AND ANDREWS P. R., 1998, *Fractal geometry in digital imaging*, AP San Diego, California, USA.

[20] VAN LEUSSEN W., *Estuarine Macroflocs*, Ph.D. Thesis, 1994, University of Utrecht.

[21] VICSEK T., 1992, *Fractal growth phenomena*, World Scientific, Singapore.

[22] WELLS M. L., GOLDBERG E. D., 1993, *Colloid aggregation in seawater*, Marine Chemical, Vol. 41, pp. 353-358.

[23] WINTERWERP J. C., 1999, *On the dynamics of high-concentrateed mud suspensions*, Ph.D. Thesis, TUDelft.

Fractal F1

d_C	Radius [pixel]	
2.07	R_{gyr}	122.5
2.00	R_{min}	149.5
2.00	$\mathbf{R_{box}}$	**150.0**
1.96	R_{hyd}	169.3
1.94	R_{ave}	180.5
1.92	R_{per}	190.3
1.89	R_{max}	211.4
1.89	R_{maj}	211.4

Fractal F2

d_C	Radius [pixel]	
8.21	R_{min}	1.0
1.92	R_{hyd}	9.7
1.25	R_{per}	47.3
1.06	R_{ave}	105.2
1.04	R_{gyr}	121.2
1.00	$\mathbf{R_{box}}$	**148.5**
0.94	R_{max}	209.3
0.94	R_{maj}	209.3

Fractal F3

d_C	Radius [pixel]	
11.61	R_{min}	1.0
1.94	R_{hyd}	31.5
1.56	R_{ave}	86.1
1.50	R_{gyr}	108.7
1.46	$\mathbf{R_{box}}$	**121.5**
1.38	R_{max}	171.1
1.38	R_{maj}	171.1
1.17	R_{per}	497.4

Fractal F4

d_C	Radius [pixel]	
2.18	R_{min}	65.2
1.98	R_{gyr}	105.5
1.96	R_{hyd}	113.3
1.90	R_{ave}	133.5
1.86	$\mathbf{R_{box}}$	**149.5**
1.81	R_{maj}	173.0
1.77	R_{max}	201.8
1.75	R_{per}	211.5

Fractal F5

d_C	Radius [pixel]	
2.16	R_{min}	74.5
2.05	R_{gyr}	96.8
1.96	R_{hyd}	126.1
1.95	R_{ave}	128.7
1.90	$\mathbf{R_{box}}$	**150.0**
1.88	R_{maj}	157.5
1.83	R_{max}	182.9
1.73	R_{per}	257.7

Fractal F6

d_C	Radius [pixel]	
2.65	R_{min}	28.7
2.03	R_{gyr}	99.6
2.02	R_{ave}	102.0
1.96	R_{hyd}	120.5
1.89	R_{maj}	148.0
1.88	$\mathbf{R_{box}}$	**148.5**
1.83	R_{max}	175.4
1.64	R_{per}	350.3

1st method

Fractal F1		
d_C	Radius [pixel]	
2.00	**R_{box}**	**150.0**
1.96	R_{min}	149.5
1.96	R_{gyr}	122.5
1.94	R_{hyd}	169.3
1.93	R_{ave}	180.5
1.92	R_{per}	190.3
1.89	R_{max}	211.4
1.89	R_{maj}	211.4

Fractal F2		
d_C	Radius [pixel]	
1.00	**R_{box}**	**148.5**
0.94	R_{max}	209.3
0.94	R_{maj}	209.3
0.94	R_{gyr}	121.2
0.94	R_{ave}	105.2
0.92	R_{per}	47.3
0.86	R_{hyd}	9.7
0.00	R_{min}	1.0

Fractal F3		
d_C	Radius [pixel]	
1.46	**R_{box}**	**121.5**
1.38	R_{max}	171.1
1.38	R_{maj}	171.1
1.35	R_{ave}	86.1
1.33	R_{gyr}	108.7
1.31	R_{hyd}	31.5
1.17	R_{per}	497.4
0.00	R_{min}	1.0

Fractal F4		
d_C	Radius [pixel]	
1.89	R_{gyr}	105.5
1.88	R_{hyd}	113.3
1.88	R_{min}	65.2
1.86	**R_{box}**	**149.5**
1.85	R_{ave}	133.5
1.81	R_{maj}	173.0
1.77	R_{max}	201.8
1.75	R_{per}	211.5

Fractal F5		
d_C	Radius [pixel]	
1.95	R_{min}	74.5
1.95	R_{gyr}	96.8
1.92	R_{hyd}	126.1
1.92	R_{ave}	128.7
1.90	**R_{box}**	**150.0**
1.88	R_{maj}	157.5
1.83	R_{max}	182.9
1.73	R_{per}	257.7

Fractal F6		
d_C	Radius [pixel]	
1.91	R_{gyr}	99.6
1.91	R_{ave}	102.0
1.90	R_{hyd}	120.5
1.88	**R_{box}**	**148.5**
1.88	R_{min}	28.7
1.88	R_{maj}	148.0
1.83	R_{max}	175.4
1.64	R_{per}	350.3

2nd method